Theoretically exact FBP-type inversion algorithm for spiral CT

Alexander Katsevich

Abstract— **Proposed is a theoretically exact formula for inversion of data obtained by a spiral CT scan with a 2-D detector array. The detector array is supposed to be of limited extent in the axial direction. The main property of the formula is that it can be implemented in a truly filtered backprojection fashion. First, one performs shift-invariant filtering of a derivative of the cone beam projections, and, second, the result is back-projected in order to form an image. Another property is that the formula solves the so-called "long object problem". Limitations of the algorithm are discussed. Results of numerical experiments are presented.**

I. Introduction

In the past decade it became clear that spiral CT can be significantly improved if one uses two-dimensional detector arrays instead of one-dimensional ones. However, accurate and efficient image reconstruction from the data provided by such scanners is very challenging because there does not exist a theoretically exact and efficient reconstruction formula. Several approaches for image reconstruction have been proposed. They can be classified into two groups: theoretically exact and approximate. See [1] for a recent review of available algorithms. Most of exact algorithms are based on computing the Radon transform for a given plane by partitioning the plane in a manner determined by the spiral path of the x-ray source [2], [3], [4], [5]. Even though exact algorithms are more accurate, they are computationally quite intensive and require keeping considerable amount of cone beam (CB) projections in memory. Approximate algorithms are much more efficient (see e.g. [6], [7], [8], [9] for several most recent techniques), but produce artifacts, which can be significant under unfavorable circumstances. Despite the progress achieved in recent years, it appears that no algorithm which would be both efficient and theoretically exact have been proposed in the literature so far.

In this paper we propose the first theoretically exact inversion formula for Spiral CT which is truly of the filtered backprojection (FBP) type. This means that the formula can be numerically implemented in two steps. First, one performs shift-invariant filtering of a derivative of the CB projections, and, second, the result is back-projected in order to form an image. The price to pay for this efficient structure is that the algorithm requires an array wider than the theoretically minimum one. Also, the algorithm is applicable if radius of support of the patient inside the gantry is not too big (not greater than $\approx 0.62\times$ radius of gantry). Clearly, this limitation is not a big problem in many cases: for example, when one scans the head or an extremity of a patient.

This research was supported in part by NSF grant DMS-9704285.
The author is with the Department of Mathematics, University of Central Florida, Orlando, FL 32816-1364. E-mail address: akatsevi@pegasus.cc.ucf.edu

II. Inversion formula

First we introduce the necessary notations. Let

$$C := \{y \in \mathbb{R}^3 : y_1 = R\cos(s), y_2 = R\sin(s), y_3 = s(h/2\pi), \\ s \in I\},\ I := [a,b], \tag{1}$$

where $h > 0, b > a$, be a spiral, and U be an open set strictly inside the spiral:

$$\overline{U} \subset \{x \in \mathbb{R}^3 : x_1^2 + x_2^2 < r^2, a(h/2\pi) < x_3 < b(h/2\pi)\}, \tag{2}$$

$0 < r < R$, S^2 is the unit sphere in $\mathbb{R}^3$, and

$$D_f(y,\beta) := \int_0^\infty f(y+\beta t)dt,\ \beta \in S^2, \tag{3}$$

$$\beta(s,x) := \frac{x - y(s)}{|x - y(s)|}, x \in U, s \in I, \tag{4}$$

$$\Pi(x,\xi) := \{y \in \mathbb{R}^3 : (y-x)\cdot\xi = 0\}, \tag{5}$$

that is $D_f(y,\beta)$ is the CB transform of f. Given $(x,\xi) \in U \times (\mathbb{R}^3 \setminus 0)$, let $s_j = s_j(\xi, \xi\cdot x), j = 1,2,\ldots,$ denote finitely many points of intersection of the plane $\Pi(x,\xi)$ with C. Also, $\dot{y}(s) := dy/ds$.

As was shown in [10], [8], any point strictly inside the spiral belongs to one and only one PI segment. Recall that a PI segment is a segment of line endpoints of which are located on the spiral and separated by less than one pitch in the axial direction. Let $s = s_b(x)$ and $s = s_t(x)$ denote values of the parameter corresponding to the endpoints of the PI segment containing x. We will call $I_{PI}(x) := [s_b(x), s_t(x)]$ the PI parametric interval. The part of the spiral corresponding to $I_{PI}(x)$ will be denoted $C_{PI}(x)$. Also, inside the PI parametric interval there exists $s_0 = s_0(x)$ such that the plane through $y(s_0)$ and parallel to $\dot{y}(s_0), \ddot{y}(s_0)$, contains x.

Fix $x \in U$. It is clear that any plane through x intersects $C_{PI}(x)$ at least at one point. Introduce the following sets:

$$\begin{aligned} Crit(x) =& \{\xi \in \mathbb{R}^3 \setminus 0 : \Pi(x,\xi) \text{ contains } y(s_b(x)), y(s_t(x)) \\ & \text{or } \Pi(x,\xi) \text{ is tangent to } C_{PI}(x)\} \cup \{0\}, \\ \Xi_1(x) =& \{\xi \in \mathbb{R}^3 : \xi \notin Crit(x) \text{ and } \Pi(x,\xi) \cap C_{PI}(x) \\ & \text{contains one point}\}, \\ \Xi_3(x) =& \mathbb{R}^3 \setminus \{\Xi_1(x) \cup Crit(x)\}. \end{aligned} \tag{6}$$

By construction, the sets $Crit(x), \Xi_{1,2}(x)$ are pairwise disjoint, their union is all of $\mathbb{R}^3$, $Crit(x)$ is closed and has Lebesgue measure zero, and $\Xi_{1,2}(x)$ are open.

Let $e_1(s,x)$ denote a unit vector in the plane through $y(s)$ and spanned by $\beta(s,x), \dot{y}(s)$ subject to the conditions that $e_1(s,x)$ is perpendicular to $\beta(s,x)$ and $e_1(s,x)\cdot\dot{y}(s) > 0$.

Given $y(s), s \in (s_b(x), s_t(x)) \setminus \{s_0(x)\}$, find $s_{tan} \in I_{PI}(x), s_{tan} \neq s$, such that the plane through $x, y(s)$, and $y(s_{tan})$ is tangent to $C_{PI}(x)$ at $y(s_{tan})$. For the exceptional values $s \in \{s_b(x), s_t(x), s_0(x)\}$, s_{tan} is determined by continuity. This construction defines a continuous function $s_{tan} = s_{tan}(s,x)$. One can show that $s = s_0(x)$ implies $s_{tan} = s_0(x)$.

Similarly, let $e_2(s,x)$ be a unit vector in the plane through $x, y(s)$, and tangent to $C_{PI}(x)$ at $y(s_{tan}(s,x))$. We require also that $e_2(s,x)$ is perpendicular to $\beta(s,x)$. This determines a continuous vector-valued function $e_2(s,x)$ up to a sign. The final requirement to eliminate ambiguity is $e_1(s,x) = e_2(s,x)$ when $s = s_{tan} = s_0(x)$.

For $f \in C_0^\infty(U)$ and $k = 1, 2$ define

$$(\mathcal{B}_k f)(x) := -\frac{1}{2\pi^2}\int_{I_{PI}(x)} \frac{1}{|x-y(s)|} \times \int_0^{2\pi} \frac{\partial}{\partial q} D_f(y(q), \cos\gamma\beta(s,x) + \sin\gamma e_k(s,x))\Big|_{q=s} \times \frac{d\gamma}{\sin\gamma} ds. \tag{7}$$

Our main result is the following theorem.

Theorem 1: The operators $\mathcal{B}_k, k = 1, 2$, can be written in the form

$$(\mathcal{B}_k f)(x) = \frac{1}{(2\pi)^3}\int_{\mathbb{R}^3} B_k(x,\xi)\tilde{f}(\xi)e^{-i\xi\cdot x}d\xi, \tag{8}$$

where for each $x \in U$, $B_k(x,\xi) \in L^\infty(\mathbb{R}^3)$ with respect to ξ and

$$B_1(x,\xi) = \begin{cases} 1, & \xi \in \Xi_1(x), \\ 3, & \xi \in \Xi_3(x), \end{cases} \quad B_2(x,\xi) = \begin{cases} 1, & \xi \in \Xi_1(x), \\ -1, & \xi \in \Xi_3(x). \end{cases} \tag{9}$$

Since the set $Crit(x)$ has Lebesgue measure zero, (9) immediately implies the following inversion formula.

Corollary 2: Under the assumptions of Theorem 1,

$$f = \frac{1}{2}(\mathcal{B}_1 f + \mathcal{B}_2 f). \tag{10}$$

An important feature of the double integral in (7) is that for each $x \in U$ the integral with respect to s is confined only to the theoretically minimal portion of the spiral $I_{PI}(x)$. This implies that inversion formula (10) solves the so-called "long object problem" (see [8] for a definition).

III. Practical implementation and numerical experiments

In this section we discuss efficient algorithms for computing $\mathcal{B}_{1,2}f$. Fix any $y(s_0)$ on the spiral. It is assumed that the detector plane is parallel to the axis of the spiral and is tangent to the cylinder $y_1^2 + y_2^2 = R^2$ (cf. (1)) at the point opposite to the source. Thus, the distance between $y(s_0)$ and the detector plane is $2R$. Stereographic projections of the upper and lower turns of the spiral onto the detector plane are denoted by Γ_{top} and Γ_{bot}, respectively (see Figures 1 and 2). Let L_0 denote the common asymptote of Γ_{top} and Γ_{bot}. The parameter Δ shown in these figures is determined by the radius of support of the patient: $\Delta = 2\cos^{-1}(r/R)$ (cf. (2)).

Fix now any $\beta \in S^2$. By construction, all points $x \in U$ such that $\beta(s,x) = \beta$ will generate the same vectors $e_1(s,x)$ and $e_2(s,x)$. Denoting the corresponding vector-valued functions by $e_1(s,\beta)$ and $e_2(s,\beta)$, rewrite $\mathcal{B}_k f, k = 1, 2$, as follows:

$$(\mathcal{B}_k f)(x) := -\frac{1}{2\pi^2}\int_{I_{PI}(x)} \frac{1}{|x-y(s)|}\Psi_k(s,\beta(s,x))ds,$$
$$\Psi_k(s,\beta) := \int_0^{2\pi} \frac{\partial}{\partial q} D_f(y(q), \cos\gamma\beta + \sin\gamma e_k(s,\beta))\Big|_{q=s} \times \frac{1}{\sin\gamma} d\gamma. \tag{11}$$

Suppose first $k = 1$. Let $\Pi(\omega), \omega \in \mathbb{R}$, denote the family of planes containing $y(s)$ and parallel to $\dot{y}(s)$. Intersections of $\Pi(\omega)$ with the detector plane generate a family of lines $L(\omega)$ parallel to L_0 (see Figure 1). Fix any $\beta \in \Pi(\omega)$. By construction, vectors $\cos\gamma\beta + \sin\gamma e_1(s,\beta), 0 \leq \gamma < 2\pi$, belong to the same plane $\Pi(\omega)$. Here, for convenience, we think of vectors $\beta, e_1(s,\beta)$, and their linear combinations as if they are attached to $y(s)$. Let θ be a polar angle in $\Pi(\omega)$. Since $e_1(s,\beta)\cdot\beta = 0, |e_1(s,\beta)| = 1$, we can write (with abuse of notation):

$$\beta = (\cos\theta, \sin\theta),\ e_1(s,\beta) = (-\sin\theta, \cos\theta), \quad \beta, e_1(s,\beta) \in \Pi(\omega). \tag{12}$$

Therefore,

$$\Psi_1(s,\beta) = \int_0^{2\pi} \frac{\partial}{\partial q} D_f(y(q), (\cos(\theta+\gamma), \sin(\theta+\gamma)))\Big|_{q=s} \times \frac{1}{\sin\gamma} d\gamma,\ \beta \in \Pi(\omega). \tag{13}$$

Equation (13) is of convolution type. Hence, one application of Fast Fourier Transform (FFT) to the integral in (13) gives values of $\Psi_1(s,\beta)$ for all $\beta \in \Pi(\omega)$ at once.

Calculation of $\mathcal{B}_2 f$ can be arranged in a similar way. Fix $s_{tan} \in [s - 2\pi + \Delta, s + 2\pi - \Delta], s_{tan} \neq s$, and let $\Pi(s_{tan})$ denote the plane through $y(s), y(s_{tan})$, and containing $\dot{y}(s_{tan})$. If $s_{tan} = s$, $\Pi(s_{tan})$ is determined by continuity and coincides with the plane through $y(s)$ and parallel to $\dot{y}(s), \ddot{y}(s)$. The family of lines $L(s_{tan})$ obtained by intersecting $\Pi(s_{tan})$ with the detector plane is shown in Figure 2. By construction, given any $x \in U$ with $\beta(s,x) \in \Pi(s_{tan})$, s_{tan} used here is precisely the

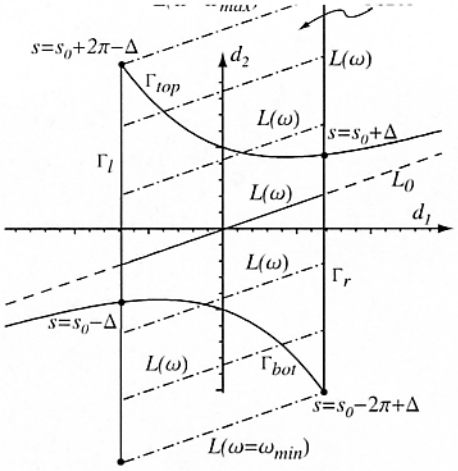

Fig. 1. Illustration of the one-parametric family of lines $L(\omega)$

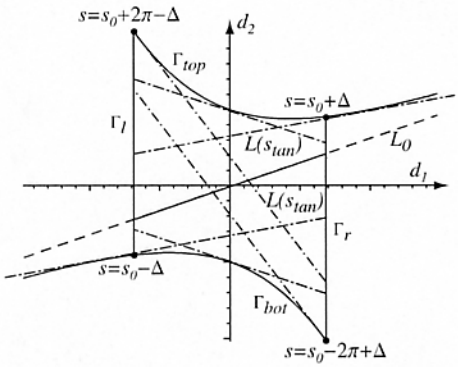

Fig. 2. Illustration of the one-parametric family of lines $L(s_{tan})$

same as s_{tan} used in the definition of $e_2(s,x)$. Since $e_2(s,\beta)\cdot\beta = 0, |e_2(s,\beta)| = 1$, we can write (with abuse of notation):

$$\beta = (\cos\theta, \sin\theta),\ e_2(s,\beta) = (-\sin\theta, \cos\theta),$$
$$\beta, e_2(s,\beta) \in \Pi(s_{tan}). \tag{14}$$

Therefore,

$$\Psi_2(s,\beta) = \int_0^{2\pi} \frac{\partial}{\partial q} D_f(y(q), (\cos(\theta+\gamma), \sin(\theta+\gamma)))\Big|_{q=s} \times \frac{1}{\sin\gamma} d\gamma,\ \beta \in \Pi(s_{tan}). \tag{15}$$

Equation (15) is of convolution type and one application of FFT gives values of $\Psi_2(s,\beta)$ for all $\beta \in \Pi(s_{tan})$ at once.

Equations (11), (13), and (15) imply that the resulting algorithm is of the filtered-backprojection type. First, one computes shift-invariant filtering of a derivative of CB projections using (13) for all required ω: $\omega_{min} \le \omega \le \omega_{max}$ (cf. Figure 1), and using (15) - for all $s_{tan} \in [s - 2\pi + \Delta, s + 2\pi - \Delta]$ (cf. Figure 2). The second step is backprojection according to the first equation in (11). Since $\partial/\partial q$ in (13) and (15) is a local operation, each CB projection is stored in memory as soon as it has been acquired for a short period of time for computing this derivative at a few nearby points and is never used later.

This discussion shows that for the algorithm to work the following two conditions must be satisfied. First, the detector array should be large enough to contain the parallelogram formed by the lines Γ_l, Γ_r and $L(\omega_{min}), L(\omega_{max})$. We will call this parallelogram the parallelogram-shaped detector array (PSDA) and its area will be denoted A_{PSDA}. Thus, the size of the detector array required for the algorithm is greater than the theoretically minimum one, which is bounded by Γ_l, Γ_r and $\Gamma_{top}, \Gamma_{bot}$. Its area will be denoted A_{min}. The ratio of the two areas is independent of the pitch h, but grows as $r \to R$. For example, $A_{PSDA}/A_{min} = 1.53$ if $r/R = 1/3$ and $A_{PSDA}/A_{min} = 1.93$ if $r/R = 0.5$. Second, the segments of lines tangent to Γ_{top} and Γ_{bot} at $s = s + 2\pi - \Delta$ and $s - 2\pi + \Delta$, respectively, and located between Γ_l and Γ_r should be inside the detector array. This requirement leads to the restriction $r/R \le \cos(\Delta_0/2) \approx 0.62$, where Δ_0 is the unique solution to the equation $\tan(2\pi - \Delta) = 2\pi - \Delta$ on the interval $\pi/2 < \Delta < \pi$.

Consider now two numerical experiments. Parameters of the data collection protocols are given in Table I.

	Shepp phantom	disk phantom
R (radius of the spiral)	3	
h (pitch of the spiral)	0.5	
axial span of the detector array	1.02	0.96
transverse span of the detector array	4.74	4.26
number of detector rows	50	
number of detectors per row	500	
number of source positions per one turn of the spiral	1500	

TABLE I
PARAMETERS OF THE DATA COLLECTION PROTOCOLS

In Figure 3 we show the results of reconstructing the 3-D low contrast Shepp phantom (see Table 1 in [11]). In the top panel we see a vertical slice through the reconstructed image at $x_1 = -0.25$, and in the bottom panel - the graphs of exact (dashed line) and computed (solid line) values of f along a vertical line $x_1 = -0.25, x_2 = 0$. We used the grey scale window $[1.01, 1.03]$ to make low-contrast features visible.

In Figure 4 we see the results of reconstructing the disk phantom, which consists of six identical flattened ellipsoids (lengths of half-axes: 0.75, 0.75, and 0.04, distance between centers of neighboring ellipsoids: 0.16). In the top panel we see a vertical slice through the reconstructed image at $x_1 = 0$, and in the bottom panel - the graphs of exact (dashed line) and computed (solid line) values of f along a vertical line $x_1 = 0, x_2 = 0$.

As one can see, the algorithm still suffers from artifacts that are due to discretization and/or sampling errors. How-

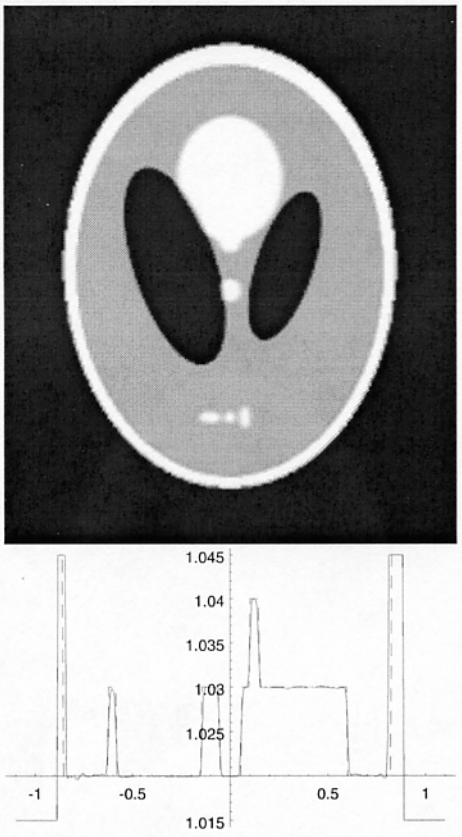

Fig. 3. Reconstruction of the 3-D Shepp phantom

ever, there are no artifacts that could be caused by non-exactness of a reconstruction scheme. Such artifacts have been theoretically studied and demonstrated numerically in [9] in the case of one approximate reconstruction algorithm. In numerical experiments presented in [9] these artifacts appear as nearly horizontal lines tangent to the ellipsoids.

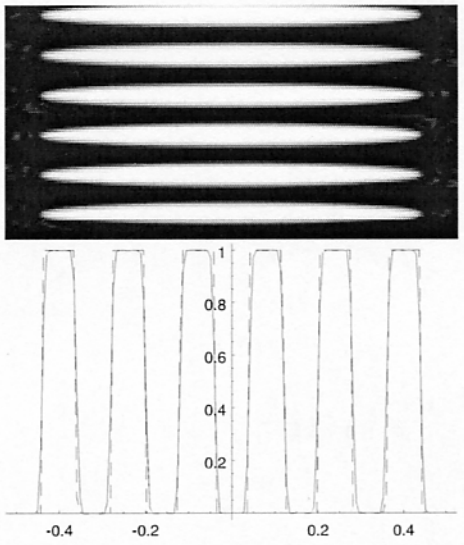

Fig. 4. Reconstruction of the disk phantom

References

[1] H. Turbell and P.-E. Danielsson, "Helical cone beam tomography," *Int. J. of Imaging Syst. and Technology*, vol. 11, pp. 91–100, 2000.

[2] K. C. Tam, "Method and apparatus for converting cone beam x-ray projection data to planar integral and reconstructing a three-dimensional computerized tomography (CT) image of an object," US Patent 5,257,183, October 1995.

[3] K. C. Tam, "Cone-beam imaging of a section of a long object with a short detector," in *Information processing in medical imaging*, J. S. Duncan and G. R. Gindi, Eds., vol. 1230 of *Lecture Notes in Computer Science*, pp. 525–530. Springer, Berlin, 1997.

[4] H. Kudo and T. Saito, "An extended cone-beam reconstruction using Radon transform," in *1996 IEEE Med. Imag. Conf. Record.* 1997, pp. 1693–1697, IEEE.

[5] S. Schaller, F. Noo, F. Sauer, et al., "Exact Radon rebinning algorithm for the long object problem in helical cone-beam CT," *IEEE Trans. on Medical Imaging*, vol. 19, pp. 361–375, 2000.

[6] H. Kudo, F. Noo, and M. Defrise, "Cone-beam filtered-backprojection algorithm for truncated helical data," *Phys. Med. Biol.*, vol. 43, pp. 2885–2909, 1998.

[7] F. Noo, H. Kudo, and M. Defrise, "Approximate short-scan filtered-backprojection for helical CB reconstruction," in *Conf. Rec. 1998 IEEE Nuclear Science Symposium*, Toronto, Ont., Canada, 1998, vol. 3, pp. 2073–2077, IEEE, Piscataway, NJ.

[8] M. Defrise, F. Noo, and H. Kudo, "A solution to the long-object problem in helical cone-beam tomography," *Physics in Medicine and Biology*, vol. 45, pp. 623–643, 2000.

[9] A. Katsevich, "Microlocal analysis of an FBP algorithm for truncated spiral cone beam data," 2000, (submitted).

[10] P. E. Danielsson et al., "Towards exact reconstruction for helical cone-beam scanning of long objects. A new detector arrangement and a new completeness condition," in *Proc. 1997 Meeting on Fully 3D Image Reconstruction in Radiology and Nuclear Medicine (Pittsburgh)*, D. W. Townsend and P. E. Kinahan, Eds., 1997, pp. 141–144.

[11] H. Kudo, N. Miyagi, and T. Saito, "A new approach to exact cone-beam reconstruction without Radon transform," in *1998 IEEE Nuclear Science Symposium Conference Record.* 1998, pp. 1636–1643, IEEE.